Electromagnetic interaction between local surface plasmon polaritons and an atmospheric surface wave plasma jet*

Chen Zhao-Quan(陈兆权)[a)†], Hu Dong(胡 东)[a)‡], Liu Ming-Hai(刘明海)[b)], Xia Guang-Qing(夏广庆)[c)], Zheng Xiao-Liang(郑晓亮)[a)], Hu Ye-Lin(胡业林)[a)], Ye Qiu-Bo(叶秋波)[a)], Chen Ming-Gong(陈明功)[a)], Zhu Long-Ji(祝龙记)[a)], and Hu Xi-Wei(胡希伟)[b)]

[a)] *College of Electrical & Information Engineering, Anhui University of Science and Technology, Huainan* 232001, *China*

[b)] *State Key Laboratory of Advanced Electromagnetic Engineering and Technology, Huazhong University of Science and Technology, Wuhan* 430074, *China*

[c)] *State Key Laboratory of Structure Analysis for Industrial Equipment, Dalian University of Technology, Dalian* 116024, *China*

(Received 25 July 2013; revised manuscript received 27 August 2013; published online 24 January 2014)

We analyze the electromagnetic interaction between local surface plasmon polaritons (SPPs) and an atmospheric surface wave plasma jet (ASWPJ) in combination with our designed discharge device. Before discharge, the excitation of the SPPs and the spatial distribution of the enhanced electric field are analyzed. During discharge, the critical breakdown electric field of the gases at atmospheric gas pressure and the surface wave of the SPPs converted into electron plasma waves at resonant points are studied. After discharge, the ionization development process of the ASWPJ is simulated using a two-dimensional fluid model. Our results suggest that the local enhanced electric field of SPPs is merely the precondition of gas breakdown, and the key mechanism in maintaining the discharge development of a low-power ASWPJ is the wave-mode conversion of the local enhanced electric field at the resonant point.

Keywords: surface wave plasma, surface plasmon polaritons, numerical simulation, electromagnetic interaction

PACS: 52.50.Sw, 52.40.Fd, 52.35.Mw, 52.25.Os **DOI:** 10.1088/1674-1056/23/3/035202

1. Introduction

Microwave discharges at atmospheric gas pressures have been investigated for a wide variety of industrial purposes. Several applications, including gas analysis, surface processing such as metal surface nitriding, gaseous waste treatments, medical instrument sterilization, and high-velocity fuel ignition, have been developed and/or improved.[1–4] Most of these applications require plasma sources that generate stable plasma glow in open air rather than confined discharge gaps. An atmospheric surface wave plasma jet (ASWPJ) is produced because it is more suitable for localized three-dimensional (3D) treatments. However, because of the difficulty in gas ionization at atmospheric gas pressure, many microwave plasma sources working in air need a higher excited microwave power for gaseous discharges, generally from kilowatts up to even megawatts.[5–11] Consequently, an important factor in the efficient discharging of the system is focused on the engineering design.

Recently, based on the local enhanced electric field of surface plasmon polaritons (SPPs), a low-power ASWPJ was obtained from gas ionization when the incident power reached 20 W.[12,13] In addition, a resonant excitation of SPPs was proposed to produce the ASWPJ. However, an alternative mechanism must be developed for the excitation of SPPs, since SPPs cannot be excited directly by an incident electromagnetic wave. In many previous studies, SPPs were excited either by creating periodical inhomogeneity on the metal surface or by placing a diffraction grating in front of the metal surface.[14–17] However, in our ASWPJ sources, only one shortened copper wire placed at the inner surface of the quartz tube can response for the excitation of SPPs and further justly with 20 W incident power, the gas discharge of the ASWPJ can come into being. In other words, the electromagnetic coupling relationship before discharge and after discharge has not been studied clearly.

The purpose of this paper is to discuss the electromagnetic interaction relationship between local SPPs and the atmospheric surface wave plasma jet. The rest of the paper is organized as follows. Before discharge, the excitation of SPPs and the spatial distribution of their enhanced electric field are analyzed in Section 2. During discharge, the critical breakdown electric field of gases at atmospheric gas pressure and surface wave mode conversion at resonant points are researched in Section 3. After discharge, using a two-dimensional (2D) fluid model, the ionization development process of the ASWPJ is simulated in Section 4. Finally, the con-

*Project supported by the National Natural Science Foundation of China (Grant No. 11105002), the Open-end Fund of State Key Laboratory of Structural Analysis for Industrial Equipment, China (Grant No. GZ1215), the Natural Science Foundation for University in Anhui Province of China (Grant No. KJ2013A106), and the Doctoral Scientific Research Funds of Anhui University of Science and Technology, China.

†Corresponding author. E-mail: zqchen@aust.edu.cn

‡Corresponding author. E-mail: austhudong@126.com

© 2014 Chinese Physical Society and IOP Publishing Ltd

clusions are summarized in Section 5.

2. The excitation of SPPs and their spatial distribution

2.1. Experimental setup and discharge experiments

In order to realize the lower power microwave discharge and the excitation of SPPs, the present study is conducted on an atmospheric pressure jet device.[12,13] Figure 1(a) shows the schematic of the jet structure. The 2.45 GHz power microwave with TE_{10} mode is through one tapered rectangular waveguide of 236 mm in length, 50 mm in height (one end) and further through a narrowed rectangular waveguide of 200 mm in length and 10 mm in height. Then, another tapered rectangular waveguide of 236 mm in length and 50 mm in height connected with a tunable short plunger at one end is joined with the narrowed rectangular waveguide at another end, which can be used to adjust the strongest electric field located at the central position of the narrowed rectangular waveguide. All the waveguides are 110 mm wide. A 5 mm radius hole is carved into the central wall of the narrowed rectangular waveguide to couple the microwave power into the quartz discharge tube. A stainless-steel sleeve, as shown in Fig. 1(a) – 45 mm long, 5 mm outer radius and 4 mm inner radius – is then placed at the upper side of the hole. The quartz tube (dielectric permittivity $\varepsilon_d = 3.78$) – 250 mm long, 4 mm outer radius and 3 mm inner radius – goes through the central hole of the metal sleeve/the waveguide, respectively. A copper wire with a radius of 0.40 mm and a length of 48 mm is set along the inner surface of the quartz tube, which is 10 mm long and below the central wall of the narrowed rectangular waveguide. The microwave power is provided by a 2.45 GHz magnetron with input power variable from 0 W to 1000 W, and equipped with a water circulator to avoid power reflection damage. Besides argon (purity of 99.999%), other gases such as helium, nitrogen, or even air can be used as the working gas. The gas flow for argon is controlled by a gas flow controller (D07-7C/ZM) with maximum flow limits of 1.0 slm (standard liter per minute). The gas flow in the discharge tube is maintained at a flow rate from 0.1 slm to 1.0 slm.

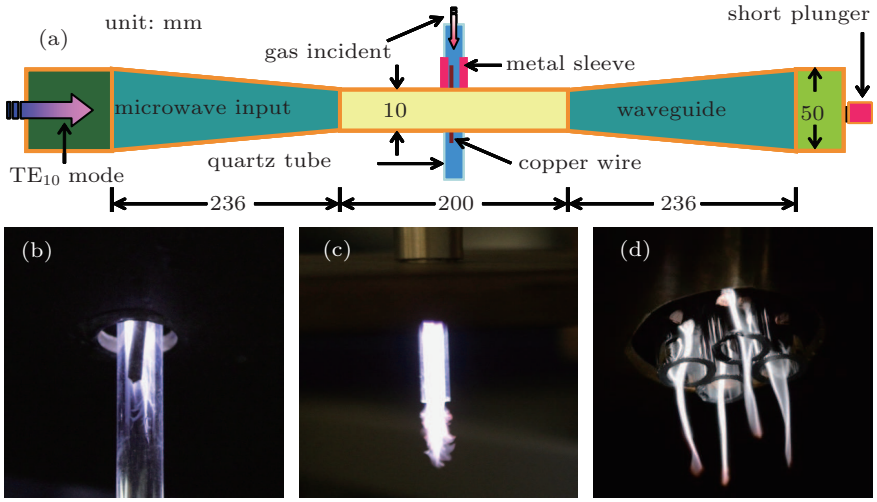


Fig. 1. (color online) (a) Schematic of the jet structure, and discharge images under different discharge conditions: (b) 20 W, 0.5 slm, (c) 90 W, 0.3 slm, and (d) 120 W, 2.4 slm.

When an input power of 20 W and argon gas flow of 0.5 slm are applied to the discharge tube, filamentary streamer discharges are generated in the whole quartz tube, as shown in Fig. 1(b). The plasma parameter can be adjusted by the gas flow rate and the applied power. When argon is injected with a gas flow rate of 0.3 slm, an input power of 90 W is applied to the discharge tube and a lightened plasma jet is generated in the whole quartz tube, as shown in Fig. 1(c). The light patterns of the jet flame in Figs. 1(b) and 1(c) show that there are several bifurcations at the end of the downstream plume, and this is called the microwave discharge mode of the filamentary streamer discharge in air.[1] In addition, a four-tube discharge array design is accomplished (as shown in Fig. 1(d)). In this new design, a stainless-steel sleeve and a narrowed rectangular waveguide are reconstructed. Using a simple case as an example, the metal sleeve has four holes and the waveguide has a larger cavity. When the total input power of 120 W is coupled into each quartz discharge tube, an argon plasma jet is equably generated in each tube. The length of the jet is about 2 cm on average, as shown in Fig. 1(d). As we know, the cross-section of the single plasma jet is typically very small, which makes large-area surface processing particularly difficult. Us-

ing plasma jet arrays may be a promising way to overcome this shortcoming. However, because of the independent characteristics of the individual plasma plumes in most cases, and the fact that they do not merge in open air, it is very difficult to achieve uniform plasmas.[18] These difficulties do not exist in our four-tube plasma jet array, as shown in Fig. 1(d), as each jet plume works independently and they seemingly attract each other. Why the discharges in our case present as expected is very interesting but complicated, and further detailed work is needed.

2.2. The excitation and spatial distribution of SPPs

In theory, SPPs produce an electromagnetic wave that propagates along the planar interface between a metal and a dielectric medium.[19–21] The surface wave of SPPs (only the transverse magnetic (TM) mode) can propagate along the interface and dissipate exponentially in spread distance. The propagation constant $k_{\rm spp}$ on the dielectric–metal interface is given by[14]

$$k_{\rm spp} = \frac{\omega}{c}\sqrt{\frac{\varepsilon_{\rm m}\varepsilon_{\rm d}}{\varepsilon_{\rm m}+\varepsilon_{\rm d}}}, \tag{1}$$

where ω is the angular frequency of the electromagnetic wave, c is the velocity of the electromagnetic wave in vacuum, $\varepsilon_{\rm m} = 1-\omega_{\rm p}^2/\left(\omega^2+{\rm i}\omega\Gamma\right)$ and $\varepsilon_{\rm d}$ are the relative permittivity of the metal and dielectric, respectively, $\omega_{\rm p} = \left[e^2N_{\rm e}/(\varepsilon_0 m_{\rm e})\right]^{1/2}$ is the angular frequency of the plasma in metal, Γ is the damping rate, and $N_{\rm e}$ is the electron density of the metal. Considering $\omega_{\rm p}/\Gamma \gg 1$ (e.g., $\omega_{\rm p} = 1.2\times10^{16}$ rad·Hz and $\Gamma = 1.45\times10^{13}$ Hz for silver in the visible frequency bands), Raether *et al.*[19] proposed some traditional approximation expressions as follows:

$$\lambda_{\rm spp} = \frac{2\pi}{k'_{\rm spp}} = \frac{2\pi c}{\omega}\left(\frac{\varepsilon_{\rm d}+\varepsilon'_{\rm m}}{\varepsilon_{\rm d}\varepsilon'_{\rm m}}\right), \tag{2}$$

for the wavelength of the SPPs and

$$\delta_{\rm spp} = \frac{1}{2k''_{\rm spp}} = \frac{\varepsilon'^{\,2}_{\rm m}c}{\varepsilon''_{\rm m}\omega}\left(\frac{\varepsilon_{\rm d}+\varepsilon'_{\rm m}}{\varepsilon_{\rm d}\varepsilon'_{\rm m}}\right)^{3/2}, \tag{3}$$

for the spread distance of the SPPs, where $\varepsilon'_{\rm m}$ and $\varepsilon''_{\rm m}$ are the real and imaginary parts of $\varepsilon_{\rm m}$, respectively. Thence, for the incident wave of ω=$2\pi\times2.45\times10^9$ Hz, the wavelength of the SPPs is about 6.0 cm (but not the wavelength in the free space of 12.25 cm). Due to the momentum between the incident wave and the surface wave of the SPPs not being consistent, the SPPs cannot be excited directly by an incident electromagnetic wave.

For the excitation of the SPPs, the wave mode conversion method should be applied. As for our discharge device, the spatial distribution of the electric fields is shown in Fig. 2. The wave mode of the incident wave in the narrowed rectangular waveguide is the $\rm TE_{10}$ mode with a wavelength of 14.9 cm, but the wave mode of the SPPs along the surface of the copper wire is the TM mode with a wavelength about 6.0 cm. Although the wave modes are different, the directions of the electric fields of the two waves have the same E_z component, which ensures that they couple with each other, as shown in Fig. 2. In order to verify the above analysis, we used HFSS (software based on the FEM method produced by ANSOFT) CAD simulation programs for 3D numerical modeling of the Maxwell equations. According to the variational principle, HFSS solving the Helmholtz equation is determined by[22]

$$F(E) = \iiint_{\Omega}\left[(\nabla\times E)\cdot(\nabla\times E) - k_0^2\varepsilon_i E^2\right]{\rm d}\Omega, \tag{4}$$

where Ω is the field of integration, and subscript i is expressed by d (dielectric) or m (metal), respectively. Here, equation (4) is the electric field governing equation in the non-source domain, and further the boundary condition that is set at the boundary and the wave excitation port established as

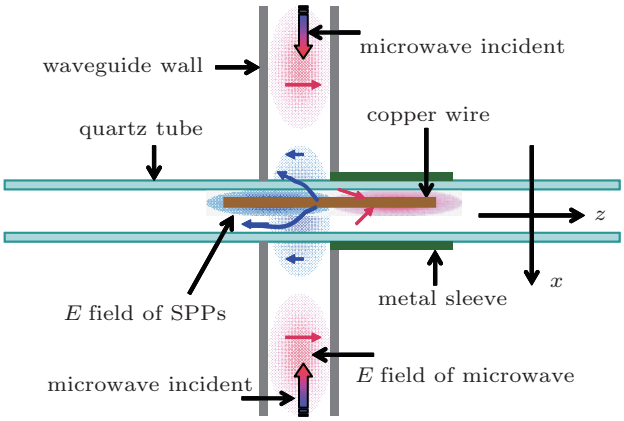


Fig. 2. (color online) The spatial distribution of the electric fields.

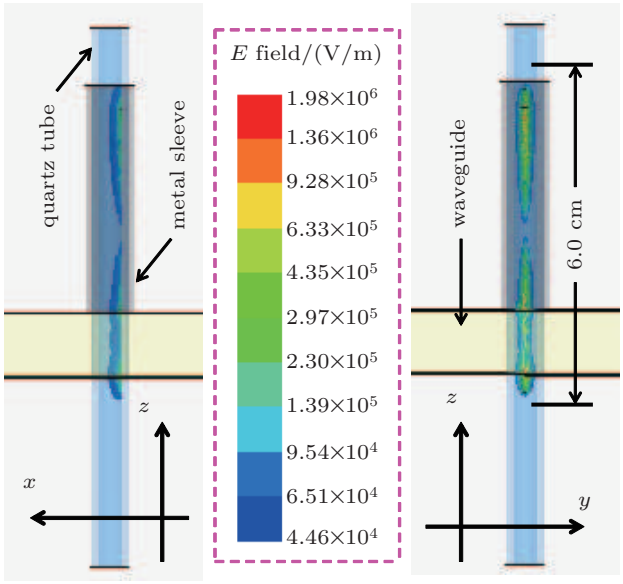


Fig. 3. (color online) The simulated electric field distribution in the discharge tube.

the driven port are adopted synchronously. The simulated model is the same as the experimental setup except without plasma (incident power of 20 W, before discharge). Figure 3 shows the E field distribution in the discharge tube. The distribution of the simulated electric field with two peaks along the quartz tube is obtained, and the wavelength scale (about 6.0 cm) is consistent with our previous theoretical calculations based on SPPs, as analyzed above.

3. The surface wave of SPPs converted into an electron plasma wave

3.1. The critical breakdown electric field of the gases

As is known, the gas is not ionized to produce plasmas until the electric field reaches the critical value of gas discharge E_c, which is in terms of[23,24]

$$E_c = 2.415 \times 10^{20} m_e (\gamma_{en}/n_N) P \sqrt{2U_i/(e^2 M)}, \quad (5)$$

where P is the gas pressure, $\gamma_{en}/n_N = 2.40 \times 10^{-13}$ m^3·s^{-1}, $U_i = 15.755$ eV, and $M = 6.634 \times 10^{-26}$ kg are the momentum transfer collision rate, ionization energy, and atom mass for argon gas at atmosphere, respectively. For nitrogen gas at atmosphere, $\gamma_{en}/n_N = 5.94 \times 10^{-13}$ m^3·s^{-1}, $U_i = 15.580$ eV, and $M = 4.683 \times 10^{-26}$ kg are the momentum transfer collision rate, ionization energy, and atom mass, respectively. For oxygen gas at atmosphere, $\gamma_{en}/n_N = 2.86 \times 10^{-13}$ m^3·s^{-1}, $U_i = 12.08$ eV, and $M = 5.352 \times 10^{-26}$ kg are the momentum transfer collision rate, ionization energy, and atom mass, respectively. Then, at atmosphere, the critical electric fields are approximately 3.0×10^5 V/m for argon, 8.9×10^5 V/m for nitrogen, and 3.1×10^5 V/m for oxygen, respectively.

Here, it should be noticed that although the critical electric field for oxygen is about 3.1×10^5 V/m, the actual breakdown electric field for pure oxygen gas is larger than 10^6 V/m, which is due to the electronegativity of oxygen. This effect can be verified by the fact that the critical electric field for air is about 3.0×10^6 V/m at atmosphere. The maximum value of the simulated E field is 1.98×10^6 V/m with an input power of 20 W, as shown in Fig. 3. Then, the maximum value of the E field is larger than the critical discharge E field of 3.0×10^5 V/m for argon. The discharge experiment also suggests that the discharge occurs as the input power is actually larger than 20 W. Hence, the discharge can occupy the region around the copper wire where the E field of the SPPs is enhanced near the metal surface.

3.2. Wave mode conversion at the resonant point

Here, the electromagnetic waves in the planar-type SW plasma sources will be analyzed. Figure 4 shows the schematics of the 2D model, which is simplified from the proposed experimental setup. We assume plasma density distributions with an up-arc parabola pattern (similar to that from the discharge measurement[25]). The function expression of the plasma density distribution can be written as

$$f(x) = 1 - (2x/d - 1)^2. \quad (6)$$

We now solve the eigenfunction for the TM modes of the SPPs. Combined with the first two curved Maxwell's equations and assuming an $\exp(-i\omega t)$ dependence for $\boldsymbol{E}$ and $\boldsymbol{B}$, we obtain[26]

$$k_{spp}^2 \frac{d}{dx} F + \left[\frac{d^2}{dx^2} + k_0^2 \varepsilon_r(x) \right] G = 0, \quad (7)$$

$$\frac{d}{dx} G + \left[k_{spp}^2 - k_0^2 \varepsilon_r(x) \right] F = 0. \quad (8)$$

In order to obtain the detailed distribution of the E field, substituting Eq. (8) into Eq. (7) obtains

$$\frac{d^2 G}{dx^2} + \frac{k_{spp}^2}{k_{spp}^2 - k_0^2 \varepsilon_r} \frac{1}{\varepsilon_r} \frac{d\varepsilon_r}{dx} \frac{dG}{dx} - \left(k_{spp}^2 - k_0^2 \varepsilon_r \right) G = 0. \quad (9)$$

To solve Eq. (9), boundary conditions are necessary. We now consider the boundary condition located at $x = 0$ in our model, as shown in Fig. 4. Here, we choose the normalization $G(x = 0) = 1$, which makes the eigenmode amplitudes E_τ independent of the excitation source.[27] As for the boundary condition placed at the location of $x = d$, the E field decreases largely, as shown in Fig. 3. For simplicity, we set $G(x = 5\ \text{mm}) = 0.05$, whose value originates from the E field located at the central position of the narrowed rectangular waveguide.

We then further consider the solutions of Eq. (9) in the plasma domain. Here, ε_r in Eq. (9) should be replaced by

$$\varepsilon_p = 1 - \frac{\omega_{p0}^2 f(x)}{\omega(\omega + i\nu_{en})},$$

and $\nu_{en} \approx 1.52 \times 10^7 P \sqrt{T_e}$ (for argon gas, T_e is the electron temperature), which is not a constant and will induce difficulty in the analytic solutions. Considering two boundary conditions at x =0 and $x = 5$ mm, we use the matrix pursuing method to solve Eq. (9) numerically. The values of F can be solved in combination with Eq. (8) as G is obtained.

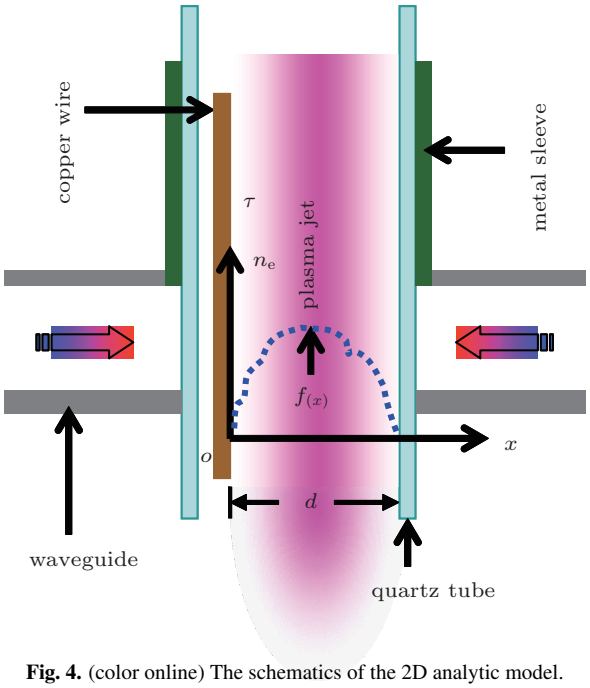


Fig. 4. (color online) The schematics of the 2D analytic model.

Figure 5 shows the results of the E field distributions, in which the maximum plasma density is assumed as 1.0×10^{18} m^{-3} and the collision rate is set according to gas pressure P. When $P = 0$ and $\nu_{en} = 0$, the amplitude distribution of the tangential electric field, which decreases from 1 to 0.05 in the plasma domain but quickly goes up to two peaks in the interim layers, is obtained, as shown in Fig. 5(a). The location of the peaks lies in the place ($\omega_p = \omega$), where the plasma density is exactly equal to 7.4×10^{16} m^{-3}. Furthermore, the amplitude distributions of the x-direction E field largely decay in both sides of the peak location, as shown in Fig. 5(b). It should be mentioned that the E field distribution near the peak position is related to the gradient distribution of the plasma density, and there are zero imaginary parts of the E field because of $\nu_{en} = 0$. Similar results can also be obtained when the input gas pressure is 10 Pa. Then, due to the existence of collision damping, imaginary parts of the E field also present near the peak points, as shown in Figs. 5(c) and 5(d). When $P = 10^5$ Pa at atmospheric pressure, the amplitude distribution of the tangential electric field, which decreases from 1 to 0.05 in the whole plasma domain, is obtained, as shown in Fig. 5(e). The amplitude distributions of the x-direction electric field decay slowly for only the real parts, but the imaginary parts decrease at two boundaries, as shown in Fig. 5(f).

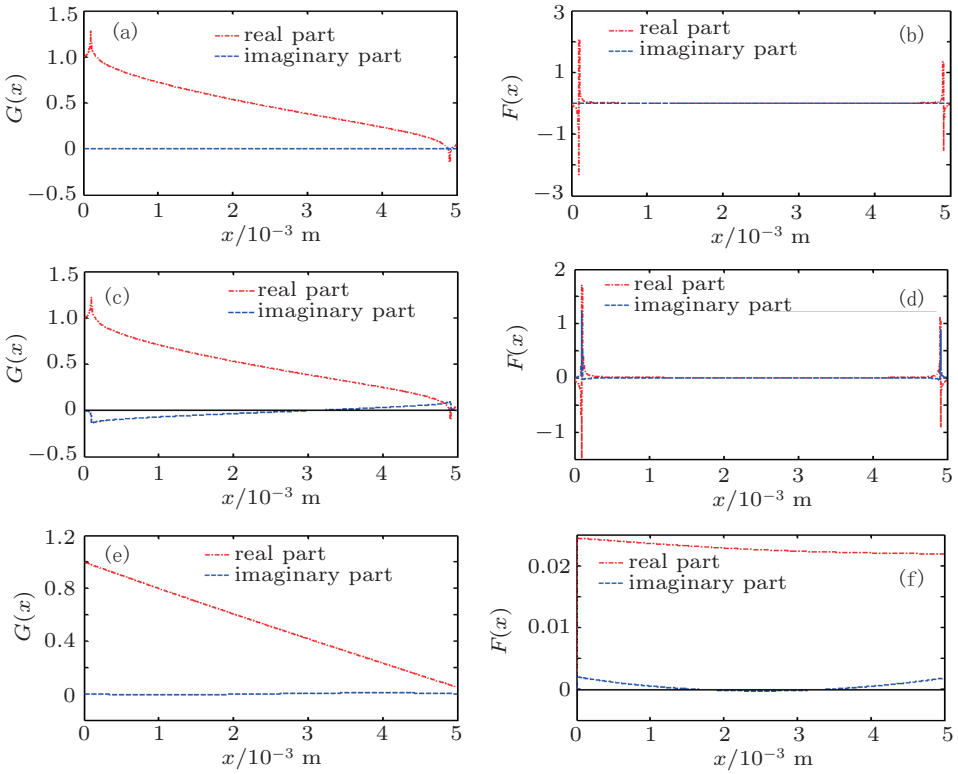


Fig. 5. (color online) The E field distribution results. (a) 0 Pa, E_τ, (b) 0 Pa, E_x, (c) 10 Pa, E_τ, (d) 10 Pa, E_x, (e) 10^5 Pa, E_τ, and (f) 10^5 Pa, E_x.

In order to study the plasma heating mechanism of the SPPs, we further analyze the wave mode conversion at the resonant point. On the one hand, the energy of the imaginary parts of the E field is damping to heat plasma directly by collisions. As shown in Fig. 5, the efficiency of this plasma heating effect is high at lower gas pressures but not at atmosphere. On the other hand, the real parts of the E field peak at lower pressures but decrease solely at atmosphere. As in our pre-

vious analysis,[28,29] the real parts of the x-direction E field can convert to electron plasma waves ($\omega^2=\omega_p^2+3\upsilon_{th}^2k^2$, υ_{th} is the electron thermal velocity) at the resonant point. After this energy conversion, the electron plasma waves propagate in the discharge domain with energy damping by collisions (Ohmic heating) or the Landau damping process.[29] Although the maximum amplitude of the real parts of the x-direction E field at atmosphere is smaller than that at lower gas pressure, the real parts of the x-direction E field at atmosphere exist in the whole plasma domain, which ensures that the wave mode conversion always occurs. Hence, wave mode conversion at the resonant point plays an important role in heating plasma to overdense states, in particular for gas discharge at atmospheric pressure.

4. Fluid simulation in the ionization development process of ASWPJ

4.1. The fluid simulation model

In contrast to the experimental investigations, numerical simulations of the discharges driven by microwave power at atmospheric pressure, such as the ionizing characteristics, have been studied less. Although the proposed discharge character has been simulated by particle-in-cell/Monte–Carlo collision models,[12] fluid simulation research on the discharge process is needed for more complete information on the plasma characteristics from starting ionization in order to reach its stable state. Here, we operate fluid simulation of the proposed plasma jet in argon gas at atmosphere.

The simulation model is a 2D fluid model developed using the COMSOL multiphysics software (version 4.2 or 4.3), which is the same as the experiments. The interaction between the plasmas and E fields is described by the fluid method,[30] and the collision processes are treated with the collision method.[31] In the initial parameter setting, the incident microwave power is applied with 20 W. The density of the initial plasmas is loaded uniformly with a density of 1.0×10^{15} m^{-3}. The background neutral gas of argon is maintained at a gas pressure of 760 Torr (1 Torr = 1.33322×10^2 Pa). The gas temperature of $T_g = 300$ K and the electron temperature of $T_e = 2.0$ eV are input as the initial temperatures. As for a detailed description of the plasma domain equations, boundary conditions, and plasma chemistry, one can refer to the MW discharge interface in the plasma module user's guide of COMSOL.[32]

4.2. The ionization development process of ASWPJ

Figure 6 shows a group of plasma electron density distributions at different time steps, 0.5 ns, 1.0 ns, 5.0 ns, 10.0 ns, 50.0 ns, 100.0 ns, 500.0 ns, and 1000.0 ns, respectively. In the time span between 1.0 ns and 5.0 ns, the ionization starts. After about 10.0 ns, the front plasma heads begin uninterrupted growth in the negative z direction. At about 500.0 ns, the pioneers of the plasma heads arrive at the domain too close to the tail of the jet plasma plume, which can be easily verified by the distribution of the electron density at 1000.0 ns, in comparison with that at 500.0 ns, as shown in Fig. 6. Figure 7 shows a group of electron temperature distributions in the working space at different time steps of 0.1 ns, 0.5 ns, 1.0 ns, 5.0 ns, 10.0 ns, 50.0 ns, 100.0 ns, and 500.0 ns, respectively. Comparing them, the longer the plasma is heated, the stronger the T_e in the domain near the end of the copper wire. In the time span between 0.1 ns and 0.5 ns, the electrons are only then accelerated, which is faster than the electron density growth. Similarly, at about 500.0 ns, the electron temperature distribution reaches its stable state.

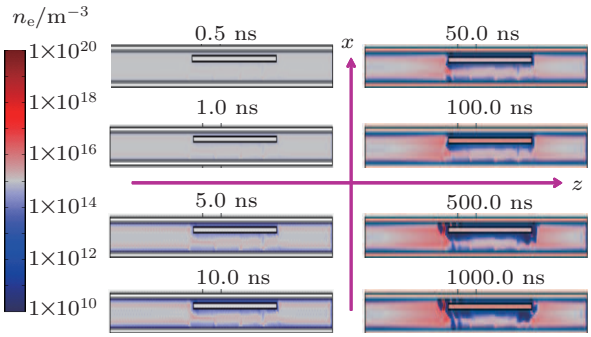


Fig. 6. (color online) Simulated plasma electron density distributions at different time steps: 0.5 ns, 1.0 ns, 5.0 ns, 10.0 ns, 50.0 ns, 100.0 ns, 500.0 ns, and 1000.0 ns, respectively.

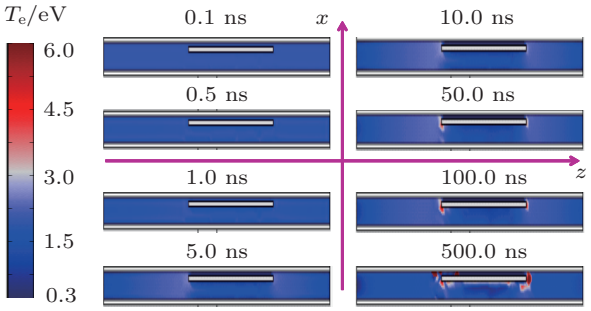


Fig. 7. (color online) Simulated electron temperature distributions at different time steps: 0.1 ns, 0.5 ns, 1.0 ns, 5.0 ns, 10.0 ns, 50.0 ns, 100.0 ns, and 500.0 ns, respectively.

It should be mentioned that the simulated discharge process occupies the domain around the copper wire, which is in good agreement with our experimental study, as shown in Figs. 1(b) and 6 (1000.0 ns). An integrated image of over eight shots in whole, the distribution of the electron density is similar to that of the photograph taken from the discharge experiment, as shown in Fig. 1(b). Figure 8 shows a group of electric field distributions at different time steps of 0.1 ns, 0.5 ns, 1.0 ns, 10.0 ns, 50.0 ns, 100.0 ns, and 500.0 ns, respectively. As shown in Fig. 8, the electric field of the SPPs exists in the time range 0.1 ns–0.5 ns, which is due to the incident wave from the excitation port to the copper wire needing about 0.33 ns (10 cm / 3×10^{10} cm/s). During the plasma

density increase, the interaction between the local SPPs and plasma enhances the local E field of the SPPs, and this interaction reaches its stable states at about 500 ns. Therefore, a conclusion can be obtained that the local enhanced E field of the SPPs plays an important role in the ionization development process of ASWPJ, comparing Figs. 6 and 7 with Fig. 8.

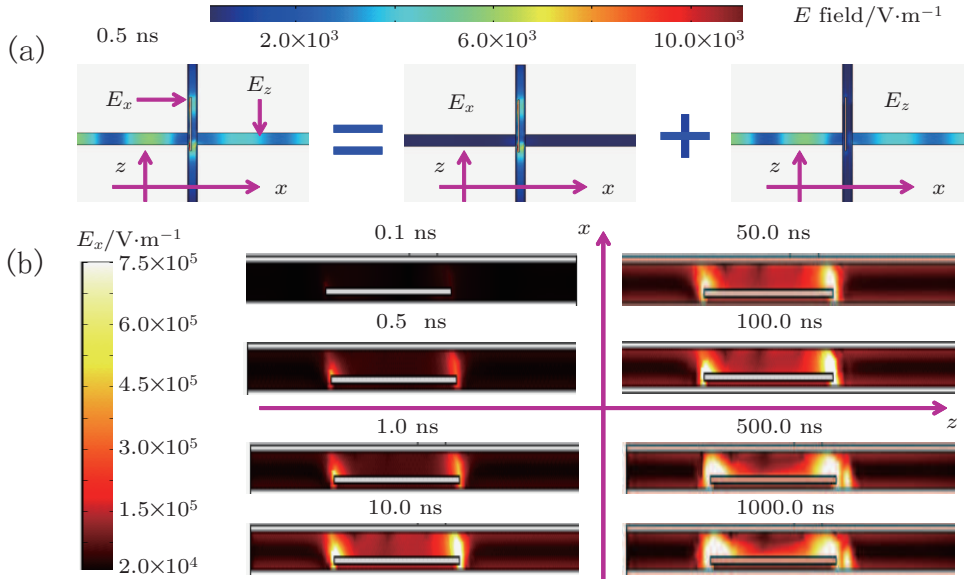


Fig. 8. (color online) Simulated electric field distributions at different time steps. (a) In the whole discharge device at a time of 0.5 ns, (b) in the discharge tube at times of: 0.1 ns, 0.5 ns, 1.0 ns, 10.0 ns, 50.0 ns, 100.0 ns, 500.0 ns, and 1000.0 ns, respectively.

In order to further study the discharge mechanism, we combine Figs. 6–8. Firstly, in our ASWPJ experimental setup, the electromagnetic wave is input into the narrowed rectangular waveguide, which excites the existence of the enhanced E field of the SPPs around the copper wire and accelerates the electrons and further ionizes the atmospheric argon gas to produce plasma. Secondly, along with the increasing density of the plasma, the surface wave of the SPPs will be converted into electron plasma waves at resonant points and disseminate the wave energy to heat the plasmas. Finally, the electrons accelerated by the enhanced electric field collide with the neutral argon atom and the density of the argon excited state atom synchronously increases. When the large-quantity argon excited state particle transmits to its atom state with lower energy, we can observe the discharge image as shown in Fig. 1(b). This is the ionization development process of ASWPJ. Moreover, it is interesting to find that the plasma growing paths all walk near the quartz surface, which may be caused by wave mode conversion at the resonant point (as shown in Fig. 5), where the diffusive loss of electrons to the dielectric walls of the column occurs, followed by the accumulation of surface charges on the dielectric walls. Thus, although it is interpreted that the discharge process produced in argon gas originates via the above assumption, further simulation or experimental works are needed to confirm this hypothesis.

5. Conclusions

In summary, this paper studies the low-power ASWPJ produced from gas ionization excited by the local enhanced electric field of SPPs, the electromagnetic coupling between before discharge and after discharge, and the electromagnetic interaction between local SPPs and the atmospheric surface wave plasma jet. Before discharge, the excitation of SPPs takes place at the surface of the copper wire, and the spatial distribution of its enhanced electric field is simulated by operating an electromagnetic simulation model. During discharge, the electromagnetic energy coupling relationship for heating plasma is analyzed, and the surface wave of SPPs converted into an electron plasma wave at resonant points plays a main role in heating plasmas. After discharge, the ionization development process of the ASWPJ is simulated using a 2D fluid model, and the discharge process reaching its stable states at a time of about 500.0 ns is obtained. The study results of this paper suggest that the local enhanced electric field of SPPs induces gas breakdown easily, and the wave mode conversion of the local enhanced electric field at the resonant point mainly determines the discharge development.

References

[1] Schlüter H and Shivarova A 2007 *Phys. Rep.* **443** 121

[2] Choi J, Iza F, Do H J, Lee J K and Cho M H 2009 *Plasma Sources Sci. Technol.* **18** 025029

[3] Takamura S, Amano S, Kurata T, Kasada H, Yamamoto J, Razzak M A, Kushida G, Ohno N and Kando M 2011 *J. Appl. Phys.* **110** 043301

[4] Aleksandrov K V, Bychkov V L, Esakov I I, Grachev L P, Khodataev K V, Ravaev A A and Matveev I B 2009 *IEEE Trans. Plasma Sci.* **37** 2293

[5] Yoshiteru H, Choi E M, Mastovsky I, Shapiro M A, Sirigiri J R and Temkin R J 2008 *Phys. Rev. Lett.* **100** 035003

[6] Jean-Pierre B, Bhaskar C and Zhu G Q 2010 *Phys. Rev. Lett.* **104** 015002

[7] Zhu G, Boeuf J P and Li J 2012 *Acta. Phys. Sin.* **61** 235202 (in Chinese)

[8] Zhou Q, Dong Z and Chen J 2011 *Acta. Phys. Sin.* **60** 125202 (in Chinese)

[9] Yang J, Shi F, Yang T and Meng Z 2010 *Acta. Phys. Sin.* **59** 8701 (in Chinese)

[10] Hubner S, Palomares J M, Carbone E A D and van der Mullen J J A M 2012 *J. Phys. D: Appl. Phys.* **45** 055203

[11] Hnilica J, Kudrle V, Vasina P, Schafer J and Aubrecht V 2012 *J. Phys. D: Appl. Phys.* **45** 055201

[12] Chen Z, Liu M, Xia G and Huang Y 2012 *IEEE Trans. Plasma Sci.* **40** 2861

[13] Chen Z, Xia G, Zhou Q, Hu Y, Zheng X, Zhen Z, Hong L, Li P and Huang Y 2012 *Rev. Sci. Instrum.* **83** 084701

[14] Xu X, Liu F, Zhou Q, Liang B, Liang Y and Liang R 2008 *Appl. Phys. Lett.* **92** 011501

[15] Wang L, Cao J, Wang Y, Niu T, Liu L and Lv Y 2008 *Chin. Phys. B* **17** 2257

[16] Chen Z, Liu M, Lan C, Chen W, Luo Z and Hu X 2008 *Chin. Phys. Lett.* **25** 4333

[17] Chen Z, Liu M, Lan C, Chen W, Tang L, Luo Z, Yan B, Lv J and Hu X 2009 *Chin. Phys. B* **18** 3484

[18] Wu S, Wang Z, Huang Q, Lu X and Ostrikov K 2012 *Phys. Plasmas* **19** 103503

[19] Agranovich V M and Mills D L 1982 *Surface Polaritions-Electromagnetic Waves at Surfaces and Interfaces* (Netherlands: Elsevier) Chaps. 1 and 9

[20] Chen Z, Liu M, Tang L, Hu P and Hu X 2009 *J. Appl. Phys.* **106** 013314

[21] Chen Z, Liu M, Tang L, Lv J, Wen Y and Hu X 2009 *J. Appl. Phys.* **106** 063304

[22] Chen Z, Liu M, Zhou Q, Hu Y, Yang A, Zhu L and Hu X 2011 *Chin. Phys. Lett.* **28** 045201

[23] Itikaza Y 1973 *Phys. Fluids* **16** 831

[24] Raizer Y P 1991 *Gas Discharge Physics* (Berlin: Springer-Verlag)

[25] Wu T J, Guan W J, Tsai C M, Yeh W Y and Kou C S 2001 *Phys. Plasmas* **8** 3195

[26] Chen Z, Liu M, Tang L, Lv J and Hu X 2010 *Chin. Phys. Lett.* **27** 025205

[27] Ghanashev I and Sugai H 2000 *Phys. Plasmas* **7** 3051

[28] Chen Z, Liu M, Hong L, Zhou Q, Cheng L and Hu X 2011 *Phys. Plasmas* **18** 013505

[29] Chen Z, Ye Q, Xia G, Hong L, Hu Y, Zheng X, Li P, Zhou Q, Hu X and Liu M 2013 *Phys. Plasmas* **20** 033502

[30] Yang A, Wang X, Rong M, Liu D, Iza F and Kong M G 2011 *Phys. Plasmas* **18** 113503

[31] Kawamura E, Graves D B and Lieberman M A 2011 *Plasma Sources Sci. Technol.* **20** 035009

[32] Chen Z, Xia G, Li P, Hong L, Hu Y, Zheng X, Wang Y, Huang Y, Zhu L and Liu M 2013 *IEEE Trans. Plasma Sci.* **41** 1658